Materials Advances

ROYAL SOCIETY OF CHEMISTRY

PAPER

View Article Online
View Journal | View Issue

Cite this: *Mater. Adv.*, 2024, 5, 9731

A superhydrophobic and heat-resistant PAN/PSU/PTFE composite nanofiber membrane for high-efficiency $PM_{1.0}$ and $PM_{2.5}$ filtration

Rizky Aflaha,[a] Chlara Naren Maharani,[b] Linda Ardita Putri,[a] Yuliyan Dwi Prabowo,[a] Iman Rahman,[a] Tarmizi Taher,[cd] Aditya Rianjanu,[de] Roto Roto,[f] Hutomo Suryo Wasisto[g] and Kuwat Triyana*[a]

Excessive particulate matter (PM) concentrations in the air can negatively impact the environment and harm human health. Hence, this issue must be addressed immediately. In this study, we developed a filtration membrane for $PM_{1.0}$ and $PM_{2.5}$ based on polyacrylonitrile/polysulfone/polytetrafluoroethylene (PAN/PSU/PTFE) composite nanofibers using an electrospinning method. Numerous characterization studies (*i.e.*, scanning electron microscopy (SEM), water contact angle (WCA) measurement, Fourier-transform infrared (FTIR) spectroscopy, tensile strength test, and thermogravimetric analysis (TGA)) were conducted to determine the surface morphology, hydrophobicity level, chemical composition, mechanical strength, and heat resistance of nanofibers, respectively. The fabricated PAN/PSU/PTFE nanofibers possess smooth and continuous morphology with sizes ranging from 270 to 407 nm, superhydrophobic surface characteristics (WCA $>$ 153°), and temperature stability at 300 °C. Furthermore, in terms of their performance as a PM filter, they demonstrate high filtration efficiency values of (99.2 $\pm$ 0.2)% and (99.3 $\pm$ 0.2)% for $PM_{1.0}$ and $PM_{2.5}$ with a pressure drop of (415 $\pm$ 5) Pa, resulting in quality factor (QF) values of (11.7 $\pm$ 0.6) $\times$ 10^{-3} Pa^{-1} and (11.9 $\pm$ 0.7) $\times$ 10^{-3} Pa^{-1}, respectively. In addition, the membrane still maintains its performance after 4 months. All these results indicate the high potential of the proposed PAN/PSU/PTFE nanofiber membrane as a PM filter in harsh environments.

Received 22nd August 2024,
Accepted 23rd October 2024

DOI: 10.1039/d4ma00841c

rsc.li/materials-advances

1. Introduction

Particulate matter (PM) is one of the most common air pollutants. PM comes from various sources (*e.g.*, vehicle emissions,[1,2] forest fires,[3–5] power plants,[6] combustion,[7,8] and industrial processes[9–11]). Based on its size, PM is divided into several categories, *i.e.*, $PM_{0.3}$ (diameter 0.3–1 μm), $PM_{1.0}$ (diameter 0.3–1 μm), $PM_{2.5}$ (diameter 1–2.5 μm), $PM_{4.0}$ (diameter 2.5–4 μm), and PM_{10} (diameter 4–10 μm).[12] The large concentration of PM in the air can negatively impact the environment, such as reducing air quality,[13,14] affecting climate change,[15,16] damaging ecosystems,[17,18] and reducing eyesight. In addition, because of its fine size, PM is not only able to enter bronchi and alveoli,[19,20] causing inflammation in the respiratory tract,[21–23] but can also lead to cardiovascular disease.[12,24,25] The estimated mortality rate affected by air pollution, mostly by $PM_{2.5}$ in 2010, was 3.15 million people.[26] Data from the World Health Organization (WHO) in 2016 indicated that 95% of the world's population lives in places with PM levels exceeding the threshold (10 $\mu g \cdot m^{-3}$).[27] Moreover, the "Global State of the Air Report 2020" stated that in 2019, there were about 6.67 million premature deaths related to indoor and outdoor air pollution.[28] All these conditions have led to an urgent requirement to not only develop real-time PM monitoring devices but also reduce PM concentrations in the air.[29–31]

Various methods have been introduced to reduce PM levels in the air, including using PM reducers (*e.g.*, cyclone dust collectors and filter bags) in PM-producing sites. Cyclone dust collectors have been proven to enable PM reduction with high efficiency, low energy consumption, and easy maintenance.[32–34] Meanwhile, filter bags provide high removal efficiency against

[a] *Department of Physics, Faculty of Mathematics and Natural Sciences, Universitas Gadjah Mada, Sekip Utara, BLS 21, Yogyakarta 55281, Indonesia. E-mail: triyana@ugm.ac.id*
[b] *Department of Physics Education, Faculty of Mathematics and Natural Sciences, Universitas Negeri Yogyakarta, Yogyakarta 55281, Indonesia*
[c] *Department of Environmental Engineering, Institut Teknologi Sumatera, Terusan Ryacudu, Way Hui, Jati Agung, Lampung Selatan 35365, Indonesia*
[d] *Center for Green and Sustainable Materials, Institut Teknologi Sumatera, Terusan Ryacudu, Way Hui, Jati Agung, Lampung 35365, Indonesia*
[e] *Department of Materials Engineering, Institut Teknologi Sumatera, Terusan Ryacudu, Way Hui, Jati Agung, Lampung 35365, Indonesia*
[f] *Department of Chemistry, Faculty of Mathematics and Natural Sciences, Universitas Gadjah Mada, Sekip Utara, BLS 21, Yogyakarta 55281, Indonesia*
[g] *PT Nanosense Instrument Indonesia, Yogyakarta 55167, Indonesia*

fine particles and high flexibility in their application.[35,36] However, both methods still have drawbacks. On the one hand, cyclone dust collectors possess low efficiency against fine particles and decreased efficiency at low airflow rates.[37,38] On the other hand, filter bags also have limitations such as high cost, complex maintenance, and unsuitability to be used in harsh environments with either extreme temperatures or very high humidity.[23]

As an alternative PM filtration method, electrospun nanofiber-based membranes have been widely developed and used considering their advantageous properties (*e.g.*, small fiber diameters, fine pores, and high filtration efficiency against PM[39–42]). The electrospinning method is often used to fabricate the nanofibers because of its simple setup preparation and proven capability to yield nanofibers with good morphologies.[39–44] Moreover, nanofibers with high heat and moisture resistance for harsh environment applications can be obtained by simply modifying hydrophobic polymer nanofiber bases with other materials having low mass degradation against temperature, resulting in composite nanofiber membranes. In previous studies, efforts have been made to compose such composite nanofibers by blending heat and moisture-resistant materials.[37,41,45,46]

In this study, we propose a novel electrospun composite nanofiber membrane by blending polyacrylonitrile (PAN) as the nanofiber base with polysulfone (PSU) and polytetrafluoroethylene (PTFE) that act as modifying materials to improve hydrophobicity and decrease mass degradation against high temperature, respectively. The high hydrophobicity of nanofibers (even up to superhydrophobic levels) can help to reduce moisture on the nanofiber, thus preventing the nanofiber from being damaged due to water absorption. In addition, good hydrophobicity has the potential to create anti-fouling and anti-clogging properties in the nanofiber membrane,[47,48] giving it a longer lifetime. Besides, high-temperature resistance also plays an important role, and it can make nanofiber-based filtration membranes have the potential to be applied to high-temperature PM-generating sources, such as vehicle exhaust (30–80 °C)[37,49,50] and coal-burning furnaces (70–180 °C).[51] For the fabricated nanofiber in this study, several characterization studies (*i.e.*, scanning electron microscopy (SEM), water contact angle (WCA) measurement, Fourier-transform infrared (FTIR) spectroscopy, tensile strength test, and thermogravimetric analysis (TGA)) were carried out to determine surface morphology, hydrophobicity level, chemical composition, mechanical strength, and heat resistance of nanofibers, respectively. Besides those basic material investigations, the fabricated PAN/PSU/PTFE nanofiber membranes were assessed in PM filtration tests to classify their filtering capabilities and long-term durability. From this research, the characteristics of the PAN/PSU/PTFE nanofiber, including its $PM_{1.0}$ and $PM_{2.5}$ filtration efficiencies, were obtained, although the conducted performance evaluations were still limited to laboratory-scale testing. Further study should include the direct assessment of the fabricated nanofiber in real environmental fields containing a more complex mixture of different PMs (*e.g.*, for applications in industrial combustion or vehicles). In addition, the batch fabrication process still needs to be developed to meet industry demands, where the reproducibility, homogeneity, and upscaling of the nanofiber-based filtration membrane in massive quantities will be the main focus areas of the next research.

2. Materials and methods

2.1. Materials

Polyacrylonitrile (PAN) powder (M_w 150 000 g mol^{-1}), polysulfone (PSU) crystals (M_w 22 000 g·mol^{-1}), *N*,*N*-dimethyl formamide (DMF), polytetrafluoroethylene (PTFE) powder (mean particle size of 6–9 μm), and 1-methyl-2-pyrrolidone (NMP) were all purchased from Sigma Aldrich, Singapore. As a PM source, potassium chloride (KCl, M_w 74.55 g·mol^{-1}) was purchased from BDH Chemicals Ltd, UK. All materials were used without any purification process.

2.2. Nanofiber fabrication

The 6 wt% PAN solution was obtained by dissolving 0.3 grams of PAN powders into 5 mL of cosolvent solutions (DMF : NMP, v : v, 4 : 1). The solution was stirred using a hot plate stirrer at 60 °C with a rotating speed of 900 rpm for 1 hour to obtain a homogeneous PAN solution. PSU crystals of 1 wt% were added to the PAN solution (denoted as PAN/PSU) and stirred with the same temperature and stirring speed for 2 hours. After the PAN/PSU solution was blended homogeneously, PTFE powders with different concentrations of 0.1 wt%, 0.3 wt%, and 0.5 wt% were added to it (denoted as PAN/PSU/PTFE.1, PAN/PSU/PTFE.2, and PAN/PSU/PTFE.3, respectively). The PAN/PSU/PTFE solution was then stirred at 60 °C at a rotating speed of 900 rpm for 3 hours until the solution was mixed uniformly. An illustration of the solution synthesis process is shown in Fig. 1a.

To fabricate the nanofibers, three different solutions (*i.e.*, PAN, PAN/PSU, and PAN/PSU/PTFE) were separately put into a 10-ml syringe (Terumo, Japan). The syringe was placed and mounted into an electrospinning machine (FM-ELS001, Fumalife, Indonesia), where strong electric fields were generated between the syringe tip and the plate collector. The plate collector was connected to the ground while the syringe tip was supplied with a positive potential. The polymer solution was electrospun with a voltage of 10 kV and a tip-to-collector distance of 15 cm at room temperature of (28.4 ± 0.1) °C (measured with a SHT31 sensor, Sensirion AG, Switzerland) for ~28 hours for a total volume of 20 mL of polymer solution for each PM filtration testing membrane. An illustration of the nanofiber fabrication process can be seen in Fig. 1b.

2.3. Nanofiber characterizations

The surface morphologies of all fabricated nanofibers (*i.e.*, PAN, PAN/PSU, and PAN/PSU/PTFE) were investigated using scanning electron microscopy (SEM, JEOL JSM-6510), where their diameter distributions and porosity were analyzed using ImageJ software based on the captured SEM images. Water contact angle (WCA) measurements were conducted to determine the wettability of the

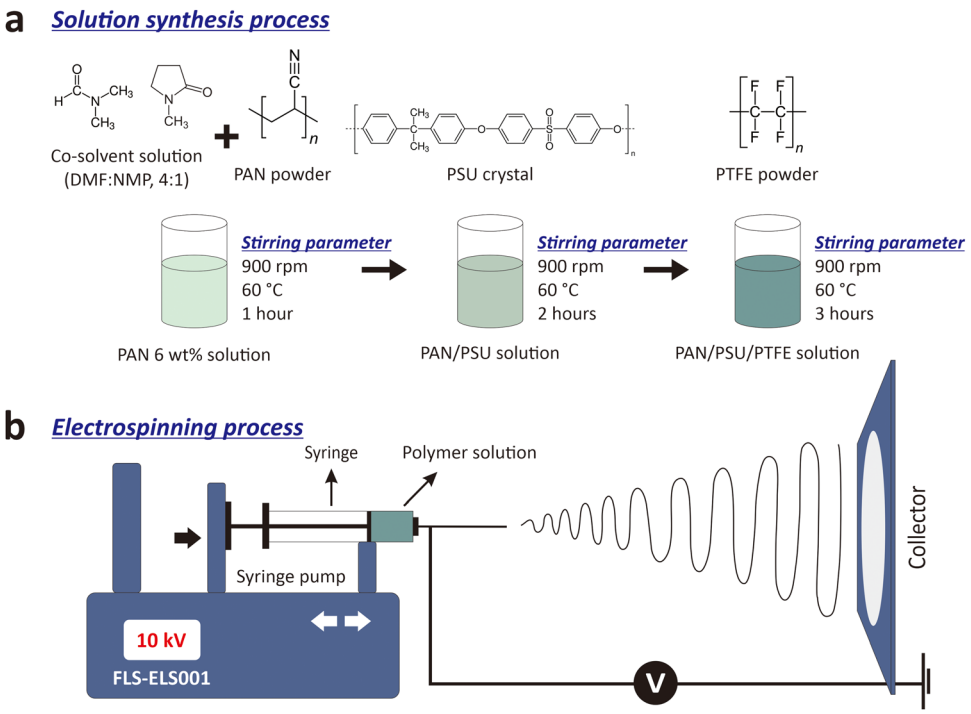

Fig. 1 **Solution synthesis and electrospinning processes to fabricate composite nanofibers**. (a) Three different solutions were prepared, *i.e.*, polyacrylonitrile (PAN), polyacrylonitrile/polysulfone (PAN/PSU), and polyacrylonitrile/polysulfone/polytetrafluoroethylene (PAN/PSU/PTFE). (b) These solutions were transformed into nanofibers using an electrospinning machine. The parameters used in the electrospinner were a voltage of 10 kV and a tip-to-collector distance of 15 cm.

nanofibers, and the WCA values were calculated using ImageJ software from images of water droplets on nanofiber membrane surfaces. Fourier-transform infrared (FTIR) spectroscopy (Thermo Nicolet iS10) was used to determine the chemical compositions of the fabricated bare PAN and composite (PAN/PSU and PAN/PSU/PTFE) nanofibers, PSU crystals, and PTFE powders. The tensile strengths of the fabricated nanofibers were measured using a motorized pull tester (Imada MX2). The mass degradation with increasing temperature of the fabricated nanofibers was observed using thermogravimetric analysis (TGA, DTG-60 Shimadzu). The filtration efficiency of nanofiber membranes against $PM_{1.0}$ and $PM_{2.5}$ and pressure drop were measured using a custom-built PM filtration setup (Nano Filtrack, Universitas Gadjah Mada, Indonesia).

2.4. PM filtration setup

Fig. 2 shows a schematic of the used PM filtration setup (Nano Filtrack, Universitas Gadjah Mada, Indonesia). The airflow was generated from an oil-less air compressor integrated with a humidity control and filter regulator unit to remove moisture, ensure air purity, and regulate air pressure and flow rate. The air was directed to the aerosol generator, where the PM source from KCl was generated. The aerosol generator comprised a 4.5-liter box with two large fans to spread the KCl powder. There were two valves connected to the aerosol generator. Valve 1 controlled airflow from the oil-less compressor to the aerosol box, and valve 2 regulated airflow to the filtration test site (FTS). A flowmeter was installed in the tube to the FTS to measure the airflow rate (liters per minute, l pm). The FTS was equipped with different sensors, *i.e.*, differential pressure and PM counter sensors. A differential pressure sensor measured the pressure drop after passing through the nanofiber-based filtration membrane. PM counter sensors measured the concentrations of $PM_{1.0}$ and $PM_{2.5}$ before and after passing through the nanofiber-based filtration membrane. A high-efficiency particulate air (HEPA) filter was installed at the end of the FTS to prevent PM from dispersing into the air.

This study used an airflow of 30 lpm and 1 gram of KCl as a PM source for one filtration process. All data obtained from the air filtration setup were stored on a personal computer (PC). The filtration efficiency (η) of the fabricated nanofiber membrane was calculated using eqn (1):

$$\eta = \left(1 - \frac{C_1}{C_0}\right) \times 100\% \quad (1)$$

where C_0 and C_1 are concentrations of the PM before and after the filtration process.[23,52,53] To comprehensively assess the overall performance of the fabricated nanofiber membranes in PM filtration, the quality factor (QF) variable was determined (eqn (2)):

$$\mathrm{QF} = -\frac{\ln(1-\eta)}{\Delta P} \quad (2)$$

where ΔP is the pressure drop.[54,55]

Different deposition methods can be used to trap PMs or particles onto such collecting materials (*e.g.*, filtering nanofiber

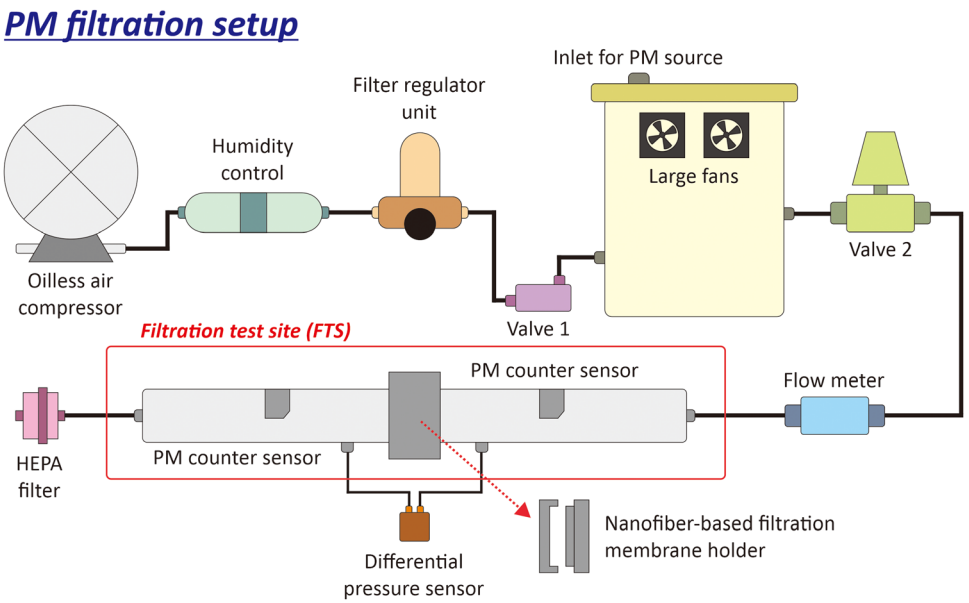

Fig. 2 **Particulate matter (PM) filtration setup**. The filtration test site (FTS) comprises different types of sensors, *i.e.*, a differential pressure sensor to measure the pressure difference of airflow after and before passing through the nanofiber-based filtration membrane and two PM counter sensors to monitor the amount of $PM_{1.0}$ and $PM_{2.5}$ before and after the filtration process. During the filtration test, potassium chloride (KCl) powder is employed as a PM source flown into the FTS.

membranes in this study), including inertial impaction,[56,57] electrostatic precipitation,[58–61] and thermophoretic separation.[62,63] Among them, our filtration test has adapted the impaction method, in which we applied neither static electricity nor temperature gradient to the membrane. Here, corona discharge is typically used to charge the particles/PMs to enhance the sampling/removal efficiency,[64–66] but was not involved in our filtering nanofiber membrane. Thus, during the filtration test, the flowing PMs were mainly impacted and subsequently collected onto the tested nanofiber membrane (see Fig. 2).

3. Results and discussion

3.1. Morphology of the PAN/PSU/PTFE nanofiber membrane

The surface morphologies of the fabricated nanofiber membranes are analyzed from the SEM images (see Fig. 3a), which were taken at two different magnifications (15 000× and 5000×, in the first and second rows, respectively). Here, the PAN nanofiber has a smooth and continuous morphology, which is in accordance with previous studies.[67–71] The addition of PSU into the PAN solution does not significantly change the morphology of the PAN/PSU nanofiber. After adding 0.1 wt% of PTFE into the PAN/PSU solution, the fabricated PAN/PSU/PTFE.1 nanofiber seems to have a larger diameter, although its morphology can be kept smooth and continuous. However, the diameter of the PAN/PSU/PTFE nanofiber has briefly decreased as the added PTFE concentration is set to be at higher values (*i.e.*, 0.3 wt% and 0.5 wt% for PAN/PSU/PTFE.2 and PAN/PSU/PTFE.3 samples, respectively).

Fig. 3b–f show the measured diameter distributions of all fabricated nanofibers (*i.e.*, PAN, PAN/PSU, PAN/PSU/PTFE.1, PAN/PSU/PTFE.2, and PAN/PSU/PTFE.3), which are analyzed using ImageJ software to validate the change in fiber diameter after the addition of PSU and PTFE into PAN solution. As depicted in Fig. 3b and c, the diameters of PAN and PAN/PSU nanofibers are found to be similar (*i.e.*, (306 ± 42) nm and (292 ± 46) nm, respectively). This result indicates an insignificant influence of PSU dopants on PAN nanofiber diameter. However, confirming its appearance in the SEM image (Fig. 3d), the PAN/PSU/PTFE.1 nanofiber diameter has been enlarged to be (407 ± 60) nm, which is larger than that before the PTFE blending. The dispersion of PTFE powder on the nanofiber is believed to be the root cause of the increase in nanofiber diameter. However, interestingly, as displayed in Fig. 3e and f, further increasing the PTFE concentration can result in smaller diameters of PAN/PSU/PTFE.2 (*i.e.*, (402 ± 64) nm) and PAN/PSU/PTFE.3 (*i.e.*, (270 ± 57) nm) nanofibers, respectively. Despite the changing diameters of nanofibers after being blended with PSU and PTFE, their sizes can still be maintained in the range of 270–407 nm (see Fig. 3g).

Fig. 3h shows the porosity measurement results of the fabricated nanofibers using the adjusted threshold method of ImageJ software. The porosity value of the nanofiber is highly dependent on its diameter size. The smaller the nanofiber size, the higher the porosity of the membrane. This statement is supported by the obtained porosity measurement results. The porosity of PAN nanofiber is 60.81% and increased to 60.93% after adding PSU. However, once PTFE has also been involved in the solution, the fabricated PAN/PSU/PTFE.1 nanofiber

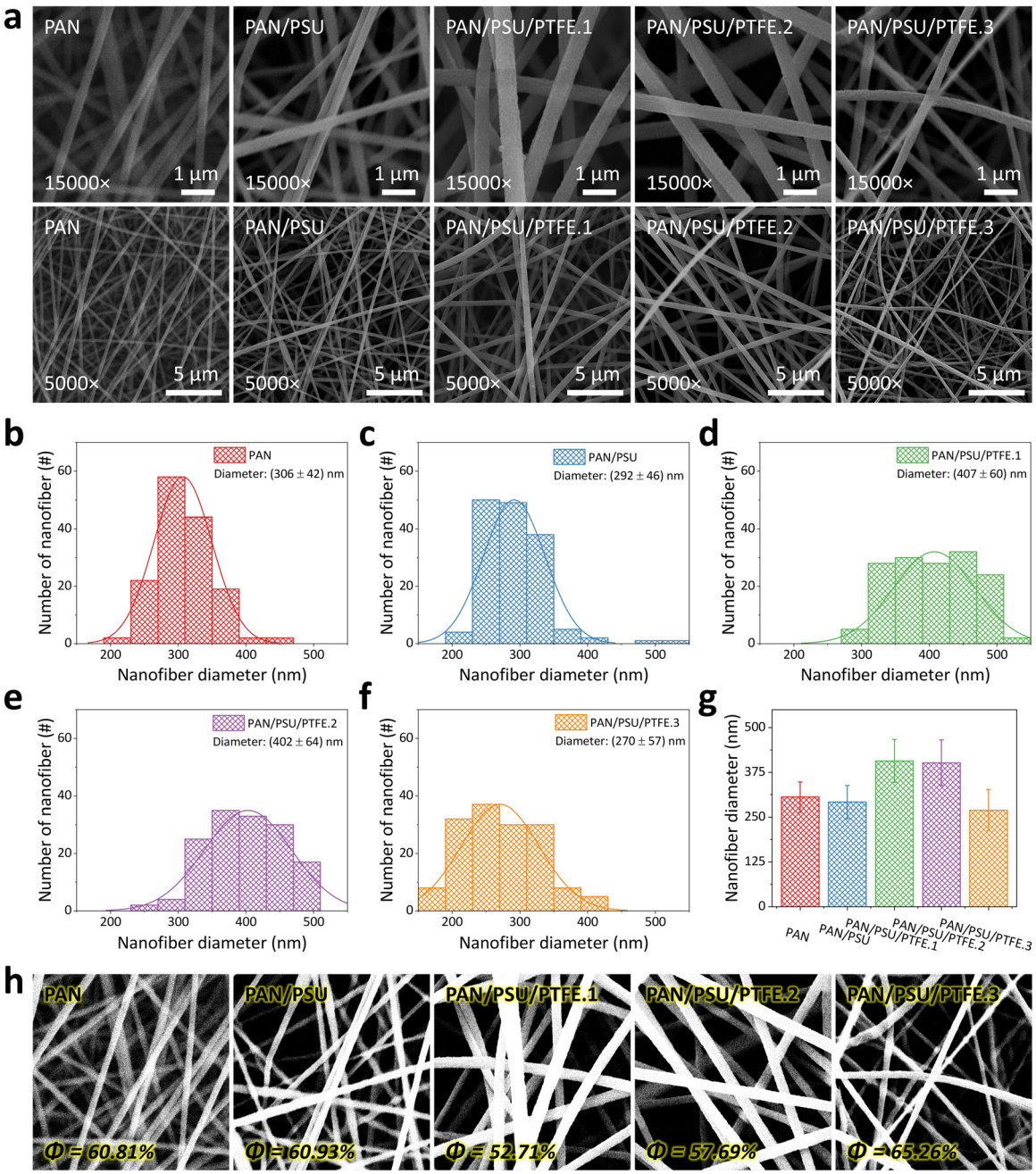

Fig. 3 **Morphology, size distribution, and porosity of the fabricated nanofiber membranes**. (a) Scanning electron microscopy (SEM) images of nanofibers with two different magnifications of 15 000× (first row) and 5000× (second row). SEM images show that all fabricated nanofibers have a smooth and continuous morphology. Diameter distributions of nanofibers analyzed using ImageJ software: (b) PAN, (c) PAN/PSU, (d) PAN/PSU/PTFE.1, (e) PAN/PSU/PTFE.2, and (f) PAN/PSU/PTFE.3 nanofibers. Significant changes in nanofiber diameter occur after the addition of PTFE. (g) Comparison of the diameter measurement results of fabricated nanofibers. (h) Porosity of the fabricated nanofibers. The PAN/PSU/PTFE.3 nanofibers experience an increase in porosity compared to PAN nanofibers.

yields a lower porosity value of 52.71%, which is attributed to the significant increase in its diameter. Meanwhile, for PAN/PSU/PTFE.2 and PAN/PSU/PTFE.3 nanofibers, their porosities are 57.69% and 65.26%, respectively. Compared to the other fabricated nanofibers, the PAN/PSU/PTFE.3 nanofiber demonstrates the highest porosity, which is affected by its smallest diameter (see Fig. 3f).

3.2. Wettability of the PAN/PSU/PTFE nanofiber membrane

The wettability of the nanofiber membrane was determined by measuring its water contact angle (WCA) value. Membrane surfaces can be categorized as having hydrophilic, hydrophobic, and superhydrophobic characteristics when they possess WCA values of $<90^\circ$, 90°–150°, and $>150^\circ$, respectively.[72] Fig. 4a shows the WCA measurement results of the fabricated

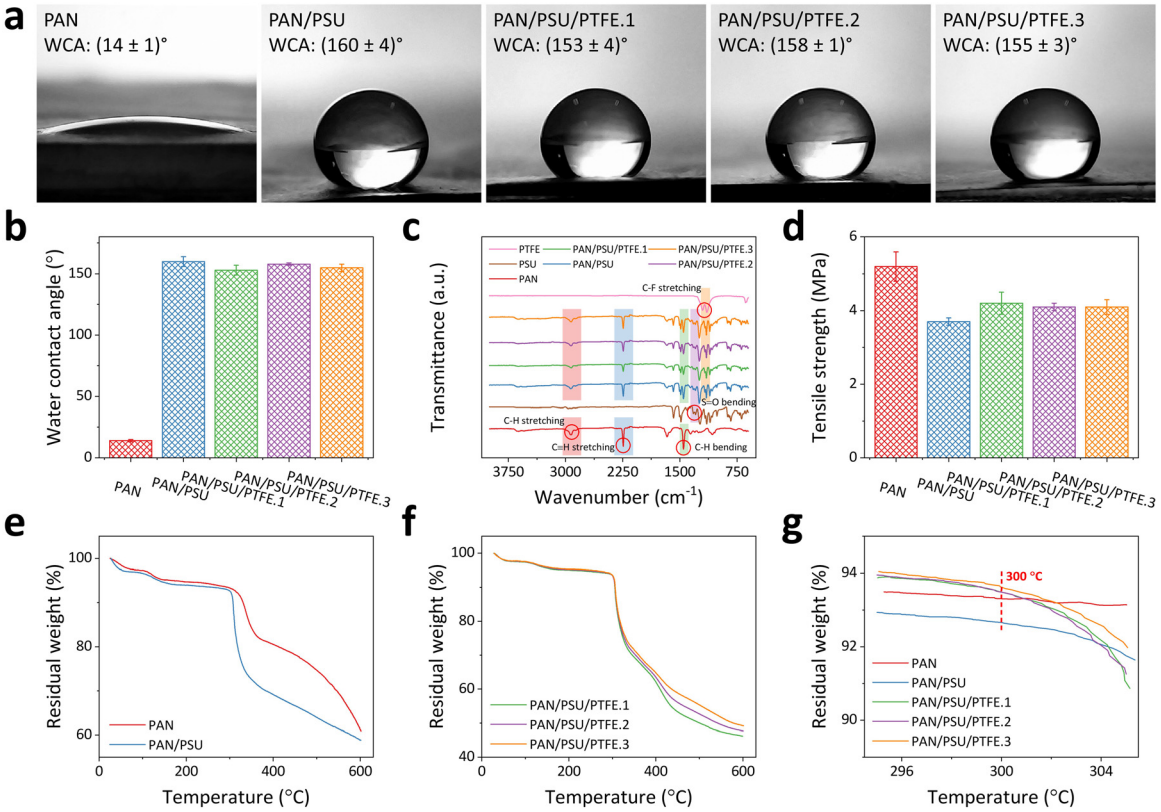

Fig. 4 **Wettability, chemical composition, mechanical strength, and heat resistance of the fabricated nanofiber membranes.** (a) Water contact angle (WCA) of fabricated nanofibers. The WCA value has increased after the addition of PSU. (b) Recapitulation of WCA of the fabricated nanofibers. (c) FTIR spectra of the PAN, PAN/PSU, PAN/PSU/PTFE nanofibers, PSU crystals, and PTFE powders. (d) The measured tensile strength of the fabricated nanofibers. PAN nanofiber obtains the highest tensile strength, while the other nanofiber variants (PAN/PSU and PAN/PSU/PTFE) exhibit similar tensile characteristics. The thermogravimetric analysis (TGA) of (e) PAN and PAN/PSU nanofibers and (f) PAN/PSU/PTFE.1, PAN/PSU/PTFE.2, and PAN/PSU/PTFE.3 nanofibers. (g) The mass percentage of fabricated nanofibers at ~300 °C. The test result shows that adding PTFE can increase the heat resistance of nanofibers up to a temperature of ~300 °C.

nanofiber membranes. Data were collected three times (n = 3), and the error value was taken from the standard deviation. Here, the PAN nanofiber has a WCA of (14 ± 1)°, indicating its hydrophilic property. Such hydrophilic surfaces are less desirable in their application as PM filtration membranes because they can easily bind water, which can reduce the lifetime of the membranes. In addition, surfaces with hydrophilic properties tend to suffer from rapid fouling and clogging.[47,48]

After the addition of PSU, there is a significant increase in WCA value to (160 ± 4)°, which can be categorized as a superhydrophobic membrane. The increase in PAN/PSU nanofiber hydrophobicity is due to the nanofiber being affected by the hydrophobic nature of PSU.[73] Here, adding only a small amount of PSU (1 wt%) to the polymer solution has sufficiently transformed the original hydrophilic surface property of PAN nanofibers to the superhydrophobic surface characteristic of PAN/PSU.[73] After adding PTFE in various concentrations of 0.1 wt% (PAN/PSU/PTFE.1), 0.3 wt% (PAN/PSU/PTFE.2), and 0.5 wt% (PAN/PSU/PTFE.3), slight decreases in their WCA values were found compared to that of the PAN/PSU nanofiber. WCA values of (153 ± 4)°, (158 ± 1)°, and (155 ± 3)° were measured for PAN/PSU/PTFE.1, PAN/PSU/PTFE.2, and PAN/PSU/PTFE.3 nanofibers, respectively. Again, although their WCA values have been lowered to some extent, the PAN/PSU/PTFE nanofiber membranes still demonstrate superhydrophobic characteristics, which are significantly different compared to a hydrophilic PAN nanofiber without PSU/PTFE blending (see Fig. 4b).

3.3. Chemical composition of the PAN/PSU/PTFE nanofiber membrane

Fig. 4c shows the FTIR spectra of all the fabricated nanofibers (*i.e.*, PAN, PAN/PSU, PAN/PSU/PTFE.1, PAN/PSU/PTFE.2, and PAN/PSU/PTFE.3), PSU crystals, and PTFE powders highlighting their typical characteristic peaks. The PAN nanofiber is seen to have peaks at 2925 cm^{-1} and 2243 cm^{-1}, suggesting the presence of C–H stretching and C≡N stretching, respectively.[74] There is also a peak at 1452 cm^{-1}, which indicates the presence of C–H bending.[68] In PSU crystals, a typical peak at 1321 cm^{-1} signifies the presence of S=O bending.[75] PAN/PSU nanofibers are expected to have a combination of peaks from PAN nanofibers and PSU crystals. The FTIR spectrum of the PAN/PSU nanofiber shows that there are peaks of C–H stretching, C≡N stretching, C–H bending, and S=O bending,[73] the same peaks found in PAN nanofiber and PSU crystals. The spectrum of PTFE powders is also presented

to investigate the effect on the chemical composition of the PAN/PSU nanofiber after adding PTFE powders. In the PTFE spectrum, there are characteristic peaks at 1200 cm^{-1} and 1145 cm^{-1}, indicating the presence of C–F stretching,[76,77] where these peaks are also slightly visible in the PAN/PSU/PTFE nanofiber. From these results, it can be validated that the PSU crystals and PTFE powders have been successfully blended into PAN nanofibers.

3.4. Mechanical strength of the PAN/PSU/PTFE nanofiber membrane

Tensile strength testing was conducted to determine the mechanical strength of the fabricated nanofibers (see Fig. 4d). The PAN nanofiber has a tensile strength of (5.2 ± 0.4) MPa. After the addition of PSU (PAN/PSU nanofiber), there is a decrease in tensile strength to (3.7 ± 0.1) MPa. The decrease in tensile strength of the nanofiber occurs due to the influence of PSU, which makes the nanofiber break more easily. From the previous study, the tensile strength of PSU was found to be lower than that of PAN.[78] However, the decrease is not too significant. In the PAN/PSU/PTFE nanofiber, there is an increase in tensile strength when compared to PAN/PSU nanofiber. The tensile strength values of PAN/PSU/PTFE.1, PAN/PSU/PTFE.2, and PAN/PSU/PTFE.3 amounted to (4.2 ± 0.3) MPa, (4.1 ± 0.1) MPa, and (4.1 ± 0.2) MPa, respectively. From the test results, it can be seen that the addition of PTFE to the nanofiber can increase its tensile strength. The tensile strength value of the PAN/PSU/PTFE nanofiber membrane was comparable to the previously reported PM filtration membrane based on an electrospun nanofiber.[79–81]

3.5. Heat resistance of the PAN/PSU/PTFE nanofiber membrane

Fig. 4e–g show the TGA results of the fabricated nanofibers. The data show the residual weight percentage of the nanofiber against increasing temperatures in the range of 25–600 °C. Fig. 4e depicts the TGA test results of PAN and PAN/PSU nanofibers to evaluate the effect of PSU addition on heat-resistant properties. Several studies have shown that PAN and PSU start to degrade in mass at ∼300 °C[82] and ∼230 °C,[83] respectively, indicating a possible decrease in the heat resistance properties of the nanofiber when PSU is added. The TGA results in Fig. 4e strengthen this statement. At 100 °C, the PAN and PAN/PSU nanofibers have 97.3% and 96.6% residual weight percentages, respectively. When the temperature was increased to 200 °C and 300 °C, the residual weight percentages of the PAN nanofiber were 94.7% and 93.3%, while those of the PAN/PSU nanofiber became 94.0% and 92.7%. Increasing the temperature to 600 °C has further lowered the remaining weight percentages of both PAN and PAN/PSU nanofibers to 61.2% and 58.9%, respectively. These results prove that the mass degradation of the PAN/PSU nanofiber is faster than that of the PAN nanofiber, which is believed to be due to the effect of the addition of PSU, which has a lower glass transition temperature (T_g) of about 185 °C.[84] Thus, even though the addition of PSU can significantly increase the hydrophobicity of the fabricated nanofiber, it has disadvantages in the heat resistance of the fabricated nanofiber. Therefore, here, we have added PTFE to solve this drawback, as a polymer that has a high melting point of 330–342 °C.[85,86]

Fig. 4f shows the mass percentage of nanofiber after the addition of PTFE (PAN/PSU/PTFE nanofiber) against increasing temperature. At 100 °C, 200 °C, and 300 °C, the mass percentages of the PAN/PSU/PTFE.1 nanofiber are 97.4%, 95%, and 93.5%, respectively, while those of the PAN/PSU/PTFE.2 nanofiber are 97.4%, 95.2%, and 93.5%, respectively. Having the largest concentration of PTFE among other fabricated composite nanofibers at those three respective temperatures, the PAN/PSU/PTFE.3 nanofiber has slightly higher mass percentages of 97.6%, 95.4%, and 93.6%. Based on these results, it can be seen that the higher the concentration of PTFE, the lower the mass degradation of the nanofiber towards increasing temperature. In other words, introducing higher PTFE concentration into the nanofiber can achieve higher heat resistance. The increased temperature resistance of the PAN/PSU/PTFE nanofiber is believed to be due to the addition of PTFE to the nanofiber, which has high heat resistance (*i.e.*, temperature stability at 500 °C).[87,88] The increased heat resistance of the fabricated nanofibers after the addition of PTFE can be seen at 300 °C (see Fig. 4g), which can already be categorized as a high temperature and is higher than the temperature of the heat flow from several PM sources, such as vehicle exhausts (30–80 °C)[37,49,50] and coal-burning furnaces (70–180 °C).[51] At 300 °C, the mass percentages of 93.3%, 92.7%, 93.5%, 93.5%, and 93.6% were measured for PAN, PAN/PSU, PAN/PSU/PTFE.1, PAN/PSU/PTFE.2, and PAN/PSU/PTFE.3 nanofibers, respectively. Here, after the addition of PTFE, the heat resistance of the nanofiber can be increased even higher than that of the PAN nanofiber while maintaining its superhydrophobic surface characteristic. Thus, the proposed PAN/PSU/PTFE nanofiber is not only superhydrophobic but also resistant to high temperatures.

3.6. $PM_{1.0}$ and $PM_{2.5}$ filtration performance of the PAN/PSU/PTFE nanofiber membrane

The filtration performance of the fabricated nanofiber membranes was tested against $PM_{1.0}$ and $PM_{2.5}$. Fig. 5a shows the efficiency of the fabricated nanofiber membranes against $PM_{1.0}$. The resulting filtration efficiency values are (98.3 ± 0.6)%, (99.3 ± 0.2)%, (98.5 ± 0.3)%, (99.2 ± 0.2)%, and (98.2 ± 1.5)% for PAN, PAN/PSU, PAN/PSU/PTFE.1, PAN/PSU/PTFE.2, and PAN/PSU/PTFE.3 nanofibers, respectively. When tested on $PM_{2.5}$, as shown in Fig. 5b, they obtain similar filtration efficiency values, which are (98.8 ± 0.1)%, (99.4 ± 0.2)%, (98.6 ± 0.3)%, (99.3 ± 0.2)%, and (98.3 ± 1.5)%, respectively. Overall, the efficiency of the fabricated nanofibers towards $PM_{2.5}$ is greater than that towards $PM_{1.0}$, as shown in Fig. 5c. The higher efficiency towards $PM_{2.5}$ occurs because $PM_{2.5}$ has a larger size than $PM_{1.0}$, making it more difficult for $PM_{2.5}$ to pass through the nanofiber membrane. Besides the filtration efficiency against PM, pressure drop (ΔP) is also one of the important parameters in PM filtration. A high-pressure drop indicates the membrane has high air resistance, resulting in poor air circulation. Therefore, a low-pressure drop is expected when designing a PM filtration membrane. From the conducted filtration tests,

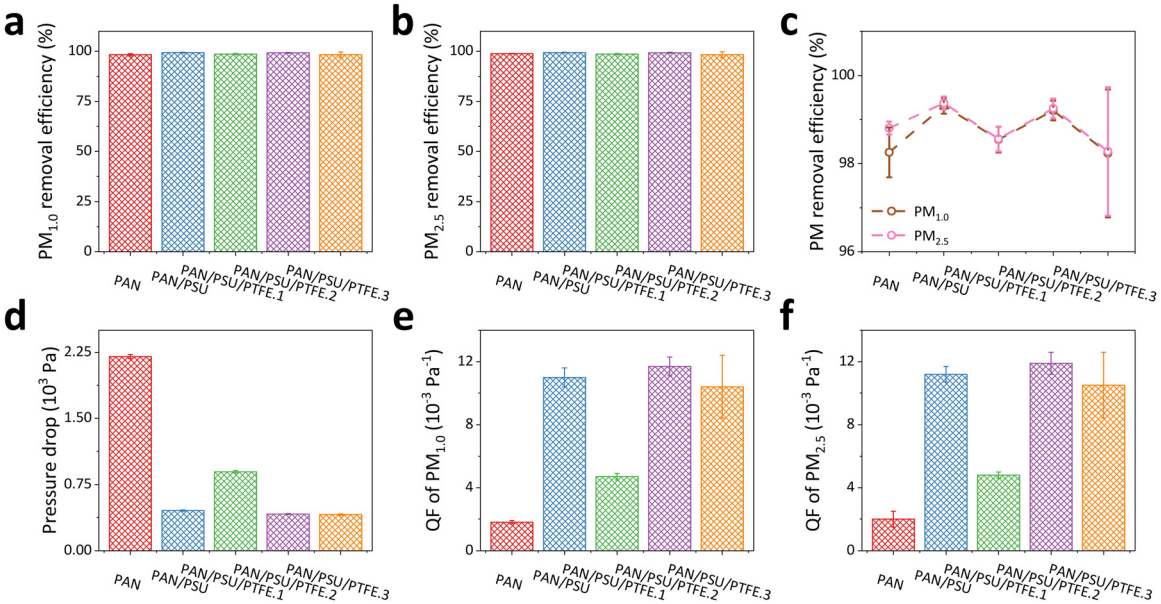

Fig. 5 **PM filtration performance of the fabricated nanofiber membranes**. The efficiency of fabricated nanofibers towards (a) $PM_{1.0}$ and (b) $PM_{2.5}$. The overall efficiency of the fabricated nanofibers is higher than 98%. (c) A comparison of the PM filtration efficiency of $PM_{1.0}$ and $PM_{2.5}$. $PM_{2.5}$ tends to have a higher efficiency because its size is larger than $PM_{1.0}$, making it more difficult to pass through the nanofiber membranes. (d) The pressure drop of the fabricated nanofibers. The PAN nanofiber has the highest pressure drop of (2200 ± 24) Pa, while the others have pressure drop values of < 895 Pa. The quality factor (QF) of (e) $PM_{1.0}$ and (f) $PM_{2.5}$. The highest QF was obtained for PAN/PSU/PTFE.2.

pressure drop values of (2200 ± 24) Pa, (453 ± 7) Pa, (895 ± 13) Pa, (415 ± 5) Pa, and (408 ± 9) Pa were found for PAN, PAN/PSU, PAN/PSU/PTFE.1, PAN/PSU/PTFE.2, and PAN/PSU/PTFE.3 nanofibers, respectively (see Fig. 5d). Here, the PAN nanofiber has the highest pressure drop among the other fabricated nanofibers. This phenomenon indicates that the air resistance of the PAN nanofiber is much higher than that of other fabricated nanofibers (PAN/PSU and PAN/PSU/PTFE nanofibers). The increase in pressure drop is prone to the hydrophobicity level of the membrane. As shown in Fig. 4a, the PAN nanofiber has a hydrophilic surface that tends to clog in high humidity because water steam cannot pass through the membrane. Meanwhile, water steam can easily penetrate the pores of the PAN/PSU and PAN/PSU/PTFE membranes and subsequently pass through them.[47]

Fig. 5e and f show the quality factor (QF) of the fabricated nanofibers against $PM_{1.0}$ and $PM_{2.5}$, respectively. The QF values are summarized in Table 1, along with the characterization test results and PM filtration test performance. Based on these values, for $PM_{1.0}$ and $PM_{2.5}$, the highest QF value belongs to the PAN/PSU/PTFE.2 nanofiber. These values indicate that the best overall performance in the filtration test performed is exhibited by PAN/PSU/PTFE.2. The best QF value can be obtained by the PAN/PSU/PTFE.2 nanofiber because it possesses both high filtration efficiencies (99.2% and 99.3% for $PM_{1.0}$ and $PM_{2.5}$, respectively) and a low-pressure drop of 415 Pa. All in all, blending of PSU crystals and PTFE powders into PAN nanofibers has been proven to be a synergistic strategy to not only result in a superhydrophobic surface and high-temperature resistant structure but also improve the PM filtration performance of the yielded membranes. Thus, the proposed composite nanofiber membranes can potentially have anti-fouling properties and be used for applications in harsh environments.

Despite its good performance, the durability of the PAN/PSU/PTFE nanofiber membrane needs to be tested to determine its

Table 1 A comparison of the key parameters for all the nanofibers fabricated in this study. The comparison includes material characteristics and the PM filtration test performance of PAN, PAN/PSU, and PAN/PSU/PTFE nanofibers

Parameter	PAN	PAN/PSU	PAN/PSU/PTFE.1	PAN/PSU/PTFE.2	PAN/PSU/PTFE.3
Nanofiber diameter (nm)	(307 ± 43)	(301 ± 63)	(405 ± 81)	(393 ± 70)	(269 ± 58)
Water contact angle (WCA) (°)	(14 ± 1)	(160 ± 4)	(153 ± 4)	(158 ± 1)	(155 ± 3)
Tensile strength (MPa)	(5.2 ± 0.4)	(3.7 ± 0.1)	(4.2 ± 0.3)	(4.1 ± 0.1)	(4.1 ± 0.2)
Nanofiber mass percentage at 300 °C (%)	93.3	92.7	93.5	93.5	93.6
Pressure drop (Pa)	(2200 ± 24)	(453 ± 7)	(895 ± 13)	(415 ± 5)	(408 ± 9)
Filtration efficiency of $PM_{1.0}$ (%)	(98.3 ± 0.6)	(99.3 ± 0.2)	(98.5 ± 0.3)	(99.2 ± 0.2)	(98.2 ± 1.5)
Quality factor (QF) of $PM_{1.0}$ (10^{-3} Pa^{-1})	(1.8 ± 0.1)	(11.0 ± 0.6)	(4.7 ± 0.2)	(11.7 ± 0.6)	(10.4 ± 2.0)
Filtration efficiency of $PM_{2.5}$ (%)	(98.8 ± 0.1)	(99.4 ± 0.2)	(98.6 ± 0.3)	(99.3 ± 0.2)	(98.3 ± 1.5)
Quality factor (QF) of $PM_{2.5}$ (10^{-3} Pa^{-1})	(2.0 ± 0.5)	(11.2 ± 0.5)	(4.8 ± 0.2)	(11.9 ± 0.7)	(10.5 ± 2.1)

performance over a long period. Fig. 6 shows the performance of the PAN/PSU/PTFE.2 nanofiber after 4 months. In terms of removal efficiency (see Fig. 6a), the performance of the PAN/PSU/PTFE.2 nanofiber did not change significantly for both $PM_{1.0}$ and $PM_{2.5}$ of (99.1 ± 0.2)% and (99.2 ± 0.2)%, respectively. These results indicate that the filtration performance of the membrane is well maintained. In another important parameter, namely pressure drop, the PAN/PSU/PTFE.2 nanofiber experienced a slight increase from (415 ± 5) Pa to (424 ± 3) Pa (see Fig. 6b). This higher pressure drop can be attributed to the influence of the already deposited PMs on the membrane from the previous filtration test. These trapped particles partially blocked the air pathways. The increase in pressure drop causes a decrease in the QF of the PAN/PSU/PTFE.2 nanofiber against $PM_{1.0}$ and $PM_{2.5}$. The QF values became (11.0 ± 0.4) 10^{-3} Pa^{-1} and (11.3 ± 0.5) 10^{-3} Pa^{-1} for $PM_{1.0}$ and $PM_{2.5}$, respectively. Despite the decrease in QF obtained, the value did not drop significantly, making it evident that it has good durability.

When compared to other PM filtration membranes from several recently reported studies, the fabricated PAN/PSU/PTFE.2 nanofiber has a competitive performance (see Table 2). This is because the high efficiency value of the fabricated PAN/PSU/PTFE.2 nanofiber, despite its high-pressure drop, gives it a less-than-optimal QF. This fabricated PAN/PSU/PTFE.2 nanofiber membrane managed to achieve high filtration efficiency values of (99.2 ± 0.2)% for $PM_{1.0}$ and (99.3 ± 0.2)% for $PM_{2.5}$, which are comparable to the research results of Xing *et al.*, who reported an efficiency of 99.9989% for $PM_{0.3}$ on a polylactic acid (PLA)-based membrane.[89] However, there is a drawback in the pressure drop of the PAN/PSU/PTFE.2 nanofiber, which reached a value of (415 ± 5) Pa, which is higher than that of Xing *et al.*, who only recorded a pressure drop of 90.35 Pa. This higher pressure drop is believed to be caused by the differences in membrane thickness or pore size, which can restrict airflow even though the filtration efficiency remains very high. When compared to the results of Amalia *et al.*,[90] which used polyvinyl chloride (PVC) waste as the base material for nanofiber membranes, our nanofiber is still superior in terms of filtration efficiency. Their $PM_{2.5}$ filtration efficiency only reached a value of 94.35%, which is still lower than that of our PAN/PSU/PTFE.2 nanofiber (>99%). However, the advantage of their membrane lies in the much lower pressure drop of 119.12 Pa, which indicates a trade-off between high filtration efficiency and air permeability in the PVC waste-based nanofiber membrane. In this case, although the PAN/PSU/PTFE.2 nanofiber has a higher pressure drop, the achieved filtration efficiency is significantly superior. In terms of QF, the PAN/PSU/PTFE.2 nanofiber showed a good performance, with QF values of (11.7 ± 0.6) × 10^{-3} Pa^{-1} for $PM_{1.0}$ and (11.9 ± 0.7) × 10^{-3} Pa^{-1} for $PM_{2.5}$. Despite the higher pressure drop, this membrane still exhibited a good balance between filtration efficiency and resistance to airflow. In comparison, the poly(vinylidene fluoride-*co*-hexafluoropropylene) PVDF–HFP-based membrane produced by Kim *et al.* has a QF of 0.0266 Pa^{-1},[91] which is comparable to the PAN/PSU/PTFE.2 nanofiber. The study by Chen *et al.* also showed outstanding filtration efficiency against nano-aerosols by using polyimide/polyethersulfone (PI/PES) nanofiber, with the highest value of 99.74% for PM 50–500 nm, yet with a very low pressure drop of only 0.98 Pa, showing great potential for applications such as face masks, where breathing comfort is an important factor.[92] Although the fabricated PAN/PSU/PTFE.2 nanofiber membrane has a comparable efficiency, the higher pressure drop could be a constraint in applications such as face masks, although it is still very competitive for use in industrial PM filtration systems. The PAN/PSU/PTFE.2 nanofiber also has a high filtration efficiency, especially against $PM_{2.5}$, which is comparable to some nanofibers in previous studies, such as a polyimide (PI) nanofiber membrane with carbon woven fabrics[93] and polyacrylonitrile-reinforced polyimide (PANNF/PI).[94] In addition, the PAN/PSU/PTFE.2 nanofiber can also be categorized as heat-resistant like the oxidized grooved and secondary pore structure poly aryl thioether sulfone (O-GPPASS) aerogel[95] and polyvinylidene fluoride (PVDF) nanofiber[96] in previous studies.

Thus, although the fabricated PAN/PSU/PTFE.2 nanofiber in this study has performed well as a PM filtration membrane, especially against $PM_{1.0}$ and $PM_{2.5}$, future research is highly recommended to overcome its shortcomings and answer the remaining questions. Several action items include the adjustment of nanofiber porosity and thickness to reduce the pressure drop and increase the QF value, the durability test to ensure the long-term use of the membrane (>4 months), the direct measurements of a nanofiber in a real environmental field comprising various PMs to evaluate its potential use in real applications, and the batch electrospinning process development to support the scale-up of the proposed

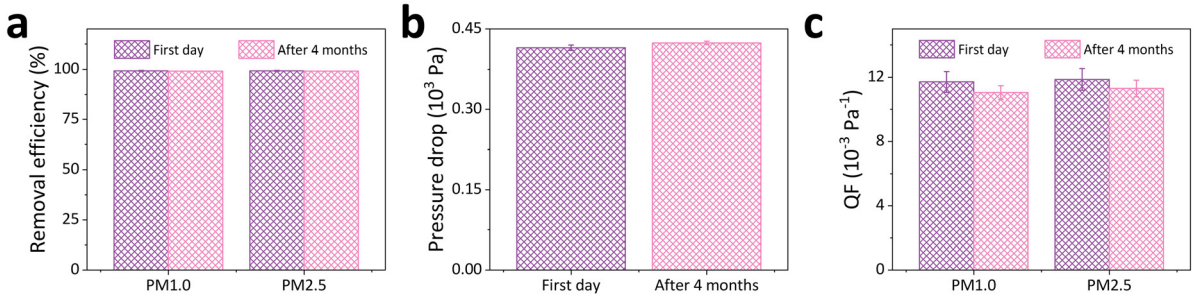

Fig. 6 **Durability of the fabricated PAN/PSU/PTFE.2 as a PM filtration membrane**. The investigated parameters to assess the membrane durability include (a) removal efficiency, (b) pressure drop, and (c) QF after 4 months. After 4 months, the membrane experienced an insignificant decrease in removal efficiency and an increase in pressure drop. Thus, there was a decrease in QF for both $PM_{1.0}$ and $PM_{2.5}$.

Table 2 PM filtration membrane performance comparison. Filtration efficiency, pressure drop, quality factor, and heat resistance are the performances highlighted in this table

Nanofiber material	Target PM size	PM filtration efficiency	Pressure drop (Pa)	Quality factor (Pa^{-1})	Heat resistant (°C)	Ref.
Polylactic acid (PLA)	$PM_{0.3}$	99.9989%	90.35	0.126	—	89
Polyvinyl chloride (PVC)	$PM_{2.5}$, $PM_{0.3}$	94.35% ($PM_{2.5}$), 94.60% ($PM_{0.3}$)	119.12	0.0245	—	90
Poly(vinylidene fluoride-*co*-hexafluoropropylene) (PVDF–HFP)	—	99.95%	~284.39	0.0266	—	91
Polyimide/polyethersulfone (PI/PES)	50-500 nm	99.74%	0.98	3.27	—	92
Polyimide (PI) nanofiber membrane with carbon woven fabrics	$PM_{2.5}$	99.99%	251.86	—	—	93
Oxidized grooved and secondary pore structure poly aryl thioether sulfone (O-GPPASS) aerogel	$PM_{0.3}$	99.7%	17.2 Pa	0.362	330	95
Polyacrylonitrile-reinforced polyimide (PANNF/PI)	$PM_{2.5}$, PM_{10}	97.2% ($PM_{2.5}$), 99.4% (PM_{10})	86.6	0.0396 ($PM_{2.5}$), 0.0567 (PM_{10})	—	94
Polyvinylidene fluoride (PVDF)	$PM_{0.3}$	97.40%	51 Pa	0.07	120 °C	96

composite nanofiber production with high reproducibility and homogeneity.

3.7. Filtration mechanisms

The effectiveness of the PAN/PSU/PTFE nanofiber in capturing PM is possible due to several mechanisms that occur between the nanofiber membrane and PM (*i.e.*, interception, inertial impaction, and Brownian diffusion), as illustrated in Fig. 7. Interception occurs because PM flowing with the airflow tends to come into direct contact with the nanofiber and is trapped due to van der Waals forces.[97,98] This mechanism tends to occur in PM with a size of 0.1–1 μm.[99] Inertial impaction occurs in PM with a larger size of 1–10 μm.[100–104] The tendency of the airflow to move at high speed and follow the porosity of the nanofiber causes PMs of large sizes to be unable to follow the movement of the airflow.[105] PM will then collide directly with the nanofiber and be trapped on its surface.[100–104] In contrast to inertial impaction, Brownian diffusion occurs in PM with a tiny size smaller than 0.1 μm.[98,106] This is because the fine PM, which flows with the airflow, tends to move with random movements generated by Brownian motion, causing it to come into contact and subsequently be trapped on the nanofiber surfaces.[107]

Besides those three mechanisms (*i.e.*, interception, inertial impaction, and Brownian diffusion), another method, the so-called electrostatic effect, is often used in filtration systems. However, this condition only applies when an electric potential is applied to the membrane so that the PM will be attracted and subsequently trapped onto the nanofiber due to the difference in charge between them.[108] In our case, we did not apply static electricity to the membrane. Thus, this electrostatic effect is not considered a governing mechanism in our PM filtration process.

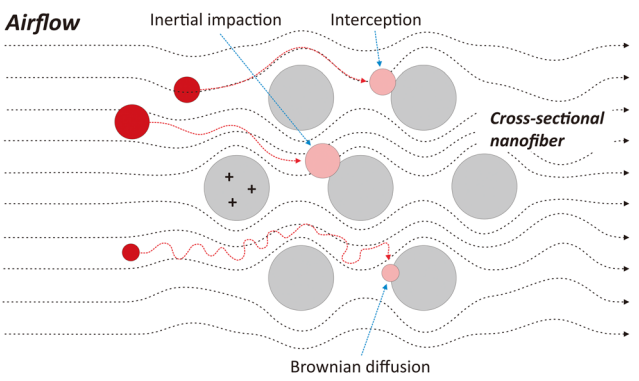

Fig. 7 **PM filtration mechanism**. Common filtration mechanisms that occur between a nanofiber and PM include interception (PM size of 0.1–1 μm), inertial impaction (PM size of 1–10 μm), and Brownian diffusion (PM size of < 0.1 μm).

4. Conclusions

The fabricated electrospun PAN/PSU/PTFE composite nanofibers have been successfully developed as high-potential $PM_{1.0}$ and $PM_{2.5}$ filtration membranes. They have diameters of (402 ± 64) nm with smooth and continuous morphology and superhydrophobic surface characteristics (WCA = (158 ± 1)°). From the obtained FTIR spectra, both PSU and PTFE have been confirmed to be present in the PAN/PSU/PTFE composite nanofiber membrane, which is indicated by their characteristic peaks in the fabricated nanofiber. Besides having a high tensile strength of (4.1 ± 0.1) MPa, the fabricated composite nanofiber membrane can maintain a mass percentage of 93.5% at 300 °C during thermogravimetric analysis (TGA) testing, which indicates its high heat resistance. In the PM filtration performance testing, the PAN/PSU/PTFE nanofiber membrane has yielded filtration efficiency values of (99.2 ± 0.2)% and (99.3 ± 0.2)% for $PM_{1.0}$ and $PM_{2.5}$, respectively. Having a pressure drop of (415 ± 5) Pa, these efficiency values can be respectively translated into QF values of (11.7 ± 0.6) × 10^{-3} Pa^{-1} and (11.9 ± 0.7) × 10^{-3} Pa^{-1}. In addition, its performance can be maintained after 4 months. Thus, the PAN/PSU/PTFE nanofiber not only has good $PM_{1.0}$ and $PM_{2.5}$ filtration performances but is also superhydrophobic and high-temperature resistant. It has been proven that a synergistic strategy (*i.e.*, blending of PSU crystals and PTFE powders into PAN nanofibers) can be

applied to not only create a superhydrophobic surface and high-temperature resistant structure of the nanofiber membrane but also improve its PM filtration performance. Thus, the proposed composite nanofiber membranes can potentially be used for applications in harsh environments. Further research should focus on finding an alternative material to PTFE because it is considered a polymer among per- and polyfluoroalkyl substance (PFAS) materials, which are most likely to be banned in the near future in several countries. In addition, performance testing of fabricated nanofibers directly in the field will be the main focus in the future to unfold their potential to be used in real filtering applications.

Author contributions

RA: conceptualization; investigation; visualization; formal analysis; writing – original draft; writing – review & editing. CNM and LAP: investigation. TT, AR, and RR: validation; formal analysis; writing – review & editing. HSW: validation; formal analysis; funding acquisition; writing – original draft; writing – review & editing. KT: conceptualization; resources; funding acquisition; supervision; formal analysis; writing – review & editing. All authors approved the final manuscript.

Data availability

The authors confirm that the data supporting the findings in this study are available within this article.

Conflicts of interest

The authors declare that there are no conflicts of interest.

Acknowledgements

This work was funded by the Ministry of Education, Culture, Research, and Technology of the Republic of Indonesia through a research scheme of ''Penelitian Kompetitif Nasional – Penelitian Pendidikan Magister menuju Doktor untuk Sarjana Unggul (PMDSU)'' under contract number of 2075/UN1/DITLIT/PT.01.03/2024. Rizky Aflaha acknowledges a PhD scholarship from the Ministry of Education, Culture, Research, and Technology of the Republic of Indonesia through the PMDSU program.

References

1 R. K. Y. Cheung, L. Qi, M. I. Manousakas, J. V. Puthussery, Y. Zheng, T. K. Koenig, T. Cui, T. Wang, Y. Ge, G. Wei, Y. Kuang, M. Sheng, Z. Cheng, A. Li, Z. Li, W. Ran, W. Xu, R. Zhang, Y. Han, Q. Wang, Z. Wang, Y. Sun, J. Cao, J. G. Slowik, K. R. Dällenbach, V. Verma, M. Gysel-Beer, X. Qiu, Q. Chen, J. Shang, I. El-Haddad, A. S. H. Prévôt and R. L. Modini, *Sci. Total Environ.*, 2024, **928**, 172345.
2 Y.-H. Ho and Y.-C. Lin, *Measurement*, 2024, **232**, 114726.
3 S. Chowdhury, R. Hänninen, M. Sofiev and K. Aunan, *Sci. Total Environ.*, 2024, **922**, 171314.
4 T. Van Do, Q. T. Vuong, E. O. Nwankwo and S.-D. Choi, *Atmos. Environ.*, 2024, **331**, 120581.
5 N. Linthoingambi Devi, A. Kumar, I. Chandra Yadav, S. Szidat and R. Sharma, *Atmos. Pollut. Res.*, 2024, **15**, 102231.
6 D. Zou, C. Zhou, Y. Gong, Z. Zhong and W. Xing, *Sep. Purif. Technol.*, 2023, **311**, 123258.
7 M. Mofijur, S. F. Ahmed, B. Ahmed, T. Mehnaz, F. Mehejabin, S. Shome, F. Almomani, A. A. Chowdhury, M. A. Kalam, I. A. Badruddin and S. Kamangar, *Energy Convers. Manage.: X*, 2024, **21**, 100515.
8 N. Nor Aznizam Nik Norizam, J. Szuhánszki, I. Ahmed, X. Yang, D. Ingham, K. Milkowski, A. Gheit, A. Heeley, L. Ma and M. Pourkashanian, *Fuel*, 2024, **374**, 132454.
9 X. Ji, Y. Yang, Y. Gou, Y. Yang, W. Li, J. Huang, W. Cai and Y. Lai, *Sep. Purif. Technol.*, 2023, **320**, 124209.
10 Y. Ren, Y. Hu and H. Cheng, *Sci. Total Environ.*, 2024, **947**, 174303.
11 Q. Yang, G. Liu, J. Falandysz, L. Yang, C. Zhao, C. Chen, Y. Sun, M. Zheng and G. Jiang, *Sci. Total Environ.*, 2024, **947**, 174467.
12 J. J. Huang, Y. Tian, R. Wang, M. Tian and Y. Liao, *Sep. Purif. Technol.*, 2020, **237**, 116377.
13 I. Manisalidis, E. Stavropoulou, A. Stavropoulos and E. Bezirtzoglou, *Front. Public Health*, 2020, 8.
14 R. D. Brook and S. Rajagopalan, *J. Am. Heart Assoc.*, 2021, **10**, e021675.
15 L. Juneng, M. T. Latif and F. Tangang, *Atmos. Environ.*, 2011, **45**, 4370–4378.
16 S. L. Fiddes, A. B. Pezza, T. A. Mitchell, K. Kozyniak and D. Mills, *Atmos. Pollut. Res.*, 2016, **7**, 1082–1089.
17 X. Luo, H. Bing, Z. Luo, Y. Wang and L. Jin, *Environ. Pollut.*, 2019, **255**, 113138.
18 D. A. Grantz, J. H. B. Garner and D. W. Johnson, *Environ. Int.*, 2003, **29**, 213–239.
19 Z. He, N. Hu, X. Meng, J. Li, Q. Wu, G. Yang, W. Zhang and Y. Wang, *Chem. Eng. J.*, 2023, **472**, 144810.
20 Q. Su, Y. Huang, Z. Wei, C. Zhu, W. Zeng, S. Wang, S. Long, G. Zhang, J. Yang and X. Wang, *Sep. Purif. Technol.*, 2023, **307**, 122652.
21 S. Zhang, H. Liu, N. Tang, N. Ali, J. Yu and B. Ding, *ACS Nano*, 2019, **13**, 13501–13512.
22 H. Liu, S. Zhang, L. Liu, J. Yu and B. Ding, *Adv. Funct. Mater.*, 2019, **26**, 1904108.
23 Y. Kang, J. Chen, S. Feng, H. Zhou, F. Zhou, Z.-X. Low, Z. Zhong and W. Xing, *J. Membr. Sci.*, 2022, **662**, 120985.
24 R. D. Arias-Pérez, N. A. Taborda, D. M. Gómez, J. F. Narvaez, J. Porras and J. C. Hernandez, *Environ. Sci. Pollut. Res.*, 2020, **27**, 42390–42404.
25 T. Xue, T. Zhu, Y. Zheng and Q. Zhang, *Nat. Commun.*, 2019, **10**, 2165.
26 J. Lelieveld, J. S. Evans, M. Fnais, D. Giannadaki and A. Pozzer, *Nature*, 2015, **525**, 367–371.
27 G. Shaddick, M. L. Thomas, H. Amini, D. Broday, A. Cohen, J. Frostad, A. Green, S. Gumy, Y. Liu, R. V. Martin,

A. Pruss-Ustun, D. Simpson, A. van Donkelaar and M. Brauer, *Environ. Sci. Technol.*, 2018, **52**, 9069–9078.
28 C. Zhou, W. Han, X. Yang, H. Fan, C. Li, L. Dong and H. Meng, *Chem. Eng. J.*, 2022, **433**, 134069.
29 H. S. Wasisto, S. Merzsch, E. Uhde, A. Waag and E. Peiner, *Microelectron. Eng.*, 2015, **145**, 96–103.
30 H. S. Wasisto, S. Merzsch, A. Waag, E. Uhde, T. Salthammer and E. Peiner, *Sens. Actuators, B*, 2013, **180**, 77–89.
31 H. S. Wasisto, E. Uhde and E. Peiner, *Build. Environ.*, 2016, **95**, 13–20.
32 P. Baltrėnas and A. Chlebnikovas, *Powder Technol.*, 2018, **333**, 327–338.
33 A. Ogawa, *J. Therm. Sci.*, 1999, **8**, 143–157.
34 P. W. Dietz, *AIChE J.*, 1981, **27**, 888–892.
35 *Environmental Pollution and Control*, ed. J. J. Peirce, R. F. Weiner, P. A. Vesilind, Butterworth-Heinemann, Woburn, 4th edn, 1998, pp. 297–313.
36 Z. Wang, *Comprehensive Energy Systems*, Elsevier, Oxford, 2018, pp. 909–949.
37 A. Zhang, H. Li, A. Zhang, J. Zhou and Y. Yan, *Compos. Commun.*, 2021, **23**, 100582.
38 H. Zhang, Y. Xie, Y. Song and X. Qin, *Colloids Surf., A*, 2021, **624**, 126831.
39 R. Aflaha, N. L. I. Sari, L. Katriani, A. H. As'ari, A. Kusumaatmaja, A. Rianjanu, R. Roto, H. S. Wasisto and K. Triyana, *Microchem. J.*, 2023, **193**, 109237.
40 R. Aflaha, L. Katriani, A. H. As'ari, N. L. I. Sari, A. Kusumaatmaja, A. Rianjanu, R. Roto and K. Triyana, *MRS Commun.*, 2023, **13**, 664–672.
41 L. Margarita Valencia-Osorio, A. Felipe Zapata-González, J. David Ojeda-Galeano, M. Lopes Aguiar and M. Lucía Álvarez-Láinez, *Sep. Purif. Technol.*, 2024, **328**, 125030.
42 Y. Deng, T. Lu, J. Cui, S. Keshari Samal, R. Xiong and C. Huang, *Sep. Purif. Technol.*, 2021, **277**, 119623.
43 R. Aflaha, H. Afiyanti, Z. N. Azizah, H. Khoirudin, A. Rianjanu, A. Kusumaatmaja, R. Roto and K. Triyana, *Biosens. Bioelectron.: X*, 2023, **13**, 100300.
44 S. A. Sofa, R. Roto, R. Aflaha, T. A. Natsir, N. A. Humairah, A. Kusumaatmaja, K. Triyana and R. Gupta, *Analyst*, 2024, **149**, 1262–1270.
45 J. Zhu, R. Zhu, Y. Hu and Z. Wang, *J. Eur. Ceram. Soc.*, 2024, **44**, 2630–2637.
46 Y. Li, D. Wang, G. Xu, L. Qiao, Y. Li, H. Gong, L. Shi, D. Li, M. Gao, G. Liu, J. Zhang, W. Wei, X. Zhang and X. Liang, *Front. Chem.*, 2021, 9.
47 X. Gao, S. Wen, B. Yang, J. Xue and H. Wang, *Chin. J. Chem. Eng.*, 2020, **28**, 1788–1795.
48 H. Fan, K. Xiao, S. Mu, Y. Zhou, J. Ma, X. Wang and X. Huang, *J. Membr. Sci.*, 2018, **556**, 312–320.
49 R. Li, J. Wu, Y. Qi and S. Zhou, *J. Alloys Compd.*, 2005, **388**, 138–144.
50 J. Galindo, R. Navarro, D. Tarí and F. Moya, *Int. J. Engine Res.*, 2020, **22**, 1540–1550.
51 Z. Li, J. Song, Y. Long, C. Jia, Z. Liu, L. Li, C. Yang, J. Liu, S. Lin, H. Wang, Y. Liu, M. Fang and H. Wu, *Nano Res.*, 2020, **13**, 861–867.
52 M. Li, Y. Feng, K. Wang, W. F. Yong, L. Yu and T.-S. Chung, *Environ. Sci. Technol.*, 2017, **51**, 10041–10049.
53 H. Souzandeh, L. Scudiero, Y. Wang and W.-H. Zhong, *ACS Sustainable Chem. Eng.*, 2017, **5**, 6209–6217.
54 Y. Li, X. Yin, J. Yu and B. Ding, *Compos. Commun.*, 2019, **15**, 6–19.
55 R. Givehchi, Q. Li and Z. Tan, *Fuel*, 2016, **181**, 1273–1280.
56 C.-H. Huang and C.-J. Tsai, *Aerosol Sci. Technol.*, 2003, **37**, 486–493.
57 X. Zhang, W. Zhang, M. Yi, Y. Wang, P. Wang, J. Xu, F. Niu and F. Lin, *Sci. Rep.*, 2018, **8**, 4757.
58 B. Pellegrin, P. Berne, H. Giraud and A. Roussey, *Indoor Air*, 2022, **32**, e12990.
59 H. S. Wasisto, S. Merzsch, E. Uhde, A. Waag and E. Peiner, *J. Sen. Sens. Syst.*, 2015, **4**, 111–123.
60 Z. Feng, Z. Long and T. Yu, *J. Electrost.*, 2016, **83**, 52–62.
61 H. S. Wasisto, S. Merzsch, A. Stranz, A. Waag, E. Uhde, T. Salthammer and E. Peiner, *Sens. Actuators, B*, 2013, **189**, 146–156.
62 H. Ström and S. Sasic, *Catal. Today*, 2012, **188**, 14–23.
63 A. Miller, A. Marinos, C. Wendel, G. King and A. Bugarski, *Aerosol Sci. Technol.*, 2012, **46**, 897–904.
64 Y. Wang, M. Yang, L. Shao, Z. Wu, W. Liu, Y. Chen, C. Zheng and X. Gao, *Sep. Purif. Technol.*, 2025, **353**, 128459.
65 T.-M. Chen, C.-J. Tsai, S.-Y. Yan and S.-N. Li, *Sep. Purif. Technol.*, 2014, **136**, 27–35.
66 C. Zheng, H. Zhang, X. Liu, Y. Wang, W. Gao, H. Zheng, D. Sun and X. Gao, *Fuel*, 2020, **278**, 118335.
67 M. Salahuddin, M. N. Uddin, G. Hwang and R. Asmatulu, *Int. J. Hydrogen Energy*, 2018, **43**, 11530–11538.
68 M. Özcan, *Phys. B*, 2024, **674**, 415584.
69 D. Wardiningsih, R. Aflaha, C. N. Maharani, K. Triyana and A. Kusumaatmaja, *Greensusmater*, 2024, **1**, 32–38.
70 A. Rianjanu, M. Aulya, M. A. A. P. Rayhan, R. Aflaha, S. Maulana, T. Taher, W. S. Sipahutar, M. I. Maulana, N. Yulianto, K. Triyana and H. S. Wasisto, *MRS Commun.*, 2023, **13**, 514–519.
71 A. Rianjanu, K. D. P. Marpaung, E. K. A. Melati, R. Aflaha, Y. G. Wibowo, I. P. Mahendra, N. Yulianto, J. Widakdo, K. Triyana, H. S. Wasisto and T. Taher, *Nano Mater. Sci.*, 2024, **6**(1), 96–105.
72 F. Sotoudeh, S. M. Mousavi, N. Karimi, B. J. Lee, J. Abolfazli-Esfahani and M. K. D. Manshadi, *Alexandria Eng. J.*, 2023, **68**, 587–609.
73 R. Aflaha, L. A. Putri, C. N. Maharani, A. Rianjanu, R. Roto, H. S. Wasisto and K. Triyana, *ACS Omega*, 2024, **9**, 29840–29847.
74 H. M. A. Hassan, I. H. Alsohaimi, M. R. El-Aassar, M. A. El-Hashemy, M. Y. El-Sayed, N. F. Alotaibi, M. A. Betiha, M. Alsuhybani and R. A. Alenazi, *Environ. Res.*, 2023, **234**, 116587.
75 A. Filimon, N. Olaru, F. Doroftei, A. Coroaba and S. Dunca, *J. Mol. Liq.*, 2021, **330**, 115664.
76 S. P. Asrafali, T. Periyasamy and S.-C. Kim, *Polymers*, 2023, 15.

77 B. He, Z. Han, J. Wang, Y. Li, J. Li, S. Song, C. Li, W. Liu and C. Wu, *J. Alloys Compd.*, 2024, **987**, 174178.
78 L. Huang, J. T. Arena, S. S. Manickam, X. Jiang, B. G. Willis and J. R. McCutcheon, *J. Membr. Sci.*, 2014, **460**, 241–249.
79 Y. Liu, C. Jia, H. Zhang, H. Wang, P. Li, L. Jia, F. Wang, P. Zhu, H. Wang, L. Yu, F. Wang, L. Wang, X. Zhang, Y. Sun and B. Li, *ACS Appl. Mater. Interfaces*, 2021, **13**, 34773–34781.
80 Q. Su, Z. Wei, C. Zhu, X. Wang, W. Zeng, S. Wang, S. Long and J. Yang, *J. Hazard. Mater.*, 2022, **431**, 128514.
81 J. Cao, Z. Cheng, L. Kang, M. Lin and L. Han, *RSC Adv.*, 2020, **10**, 20155–20161.
82 Y. Furushima, R. Kumazawa, Y. Yamaguchi, N. Hirota, K. Sawada, M. Nakada and M. Murakami, *Polymer*, 2021, **226**, 123780.
83 A. M. Alosaimi, *Polymers*, 2021, 13.
84 M. T. DeMeuse, *High Temperature Polymer Blends*, Woodhead Publishing, 2014, pp. 165–173.
85 R. G. Hill, in *BiomaterialsArtificial Organs and Tissue Engineering*, ed. L. L. Hench, J. Raman and B. Jones, Woodhead Publishing, 2005, pp. 97–106.
86 F. Macedonio, A. Ali and E. Drioli, *Comprehensive Membrane Science and Engineering*, ed. E. Drioli, L. Giorno, Elsevier, Oxford, 2nd edn, 2017, pp. 282–296.
87 S. Thomas, J. Kavil and A. Mathew Malayil, *J. Mater. Sci.: Mater. Electron.*, 2016, **27**, 9780–9788.
88 C. Pan, K. Kou, Q. Jia, Y. Zhang, Y. Wang, G. Wu and A. Feng, *J. Mater. Sci.: Mater. Electron.*, 2016, **27**, 11909–11916.
89 J. Xing, W. Zhang, S. Sun and Z. Liu, *RSC Adv.*, 2024, **14**, 14857–14867.
90 R. Amalia, A. Noviyanto, L. A. Rahma, A. Labanni, M. Fahroji, S. Purwajanti, D. A. Hapidin and A. Zulfi, *Sustainable Mater. Technol.*, 2024, **40**, e00928.
91 C. Kim, S. Hong, E. Ku, H. J. Oh, B. Jeon, H. Lee, H. Ahn, J. Choi, J. Bae, Y. O. Choi and B.-S. Lee, *J. Ind. Eng. Chem.*, 2024, DOI: **10.1016/j.jiec.2024.07.004**.
92 H.-W. Chen, Y.-L. Kuo, C.-H. Chen, C.-S. Chiou, W.-T. Chen and Y.-H. Lai, *Process Saf. Environ. Prot.*, 2022, **167**, 695–707.
93 Q. Wang, Y. Bai, J. Xie, Q. Jiang and Y. Qiu, *Powder Technol.*, 2016, **292**, 54–63.
94 X. Zhao, K. Ruan, H. Qiu, Y. Zhang and J. Gu, *Compos. Sci. Technol.*, 2023, **244**, 110275.
95 Q. Su, C. Zhu, A. Gong, S. Long, G. Zhang, Z. Wei, X. Wang and J. Yang, *Sep. Purif. Technol.*, 2024, **347**, 127573.
96 T. T. Bui, M. K. Shin, S. Y. Jee, D. X. Long, J. Hong and M.-G. Kim, *Colloids Surf., A*, 2022, **640**, 128418.
97 Y. Zhou, Y. Liu, M. Zhang, Z. Feng, D.-G. Yu and K. Wang, *Nanomaterials*, 2022, 12.
98 F. Russo, R. Castro-Muñoz, S. Santoro, F. Galiano and A. Figoli, *J. Environ. Chem. Eng.*, 2022, **10**, 108452.
99 C. Wang and Y. Otani, *Ind. Eng. Chem. Res.*, 2013, **52**, 5–17.
100 C. Darquenne, *J. Aerosol Med. Pulm. Drug Delivery*, 2014, **27**, 170–177.
101 M. Zhu, J. Han, F. Wang, W. Shao, R. Xiong, Q. Zhang, H. Pan, Y. Yang, S. K. Samal, F. Zhang and C. Huang, *Macromol. Mater. Eng.*, 2017, **302**, 1600353.
102 R. S. Barhate and S. Ramakrishna, *J. Membr. Sci.*, 2007, **296**, 1–8.
103 D. Zhang, *Ultra-supercritical coal power plants*, Woodhead Publishing, 2013, pp. 133–183.
104 H. Liu, Y. Zhu, C. Zhang, Y. Zhou and D.-G. Yu, *Nano Today*, 2024, **55**, 102161.
105 B. G. Miller, *Clean Coal Engineering Technology*, Butterworth-Heinemann, 2nd edn, 2017, pp. 419–465.
106 G. Q. Gu, C. B. Han, C. X. Lu, C. He, T. Jiang, Z. L. Gao, C. J. Li and Z. L. Wang, *ACS Nano*, 2017, **11**, 6211–6217.
107 H. K. Shin, C. Kim, P. Talkner and E. K. Lee, *Chem. Phys.*, 2010, **375**, 316–326.
108 E. Tian, Y. Gao and J. Mo, *Build. Environ.*, 2023, **228**, 109782.